



OPEN

Nanofibrous asymmetric collagen/curcumin membrane containing aspirin-loaded PLGA nanoparticles for guided bone regeneration

Mohammad Ali Ghavimi^{1,6}, Amirhossein Bani Shahabadi^{1,6}, Seyedhosein Jarolmasjed², Mohammad Yousef Memar³, Solmaz Maleki Dizaj⁴✉ & Simin Sharifi^{4,5}✉

The goal of the current study was to develop an asymmetric guided bone regeneration (GBR) membrane benefiting from curcumin and aspirin. The membrane was prepared using electrospinning technique and then was physic-chemically characterized by the conventional methods. The release profile of aspirin from the prepared membrane was also measured by ultraviolet spectrophotometry. Also, the antibacterial activities of the membrane was evaluated. We also assessed the in vitro effects of the prepared membrane on the biocompatibility and osteogenic differentiation of dental pulp stem cells (DPSCs), and evaluated in vivo bone regeneration using the prepared membrane in the defects created in both sides of the dog's jaw by histology. The results from the characterization specified that the membrane was successfully prepared with monodispersed nanosized fibers, uniform network shaped morphology, negative surface charge and sustained release platform for aspirin. The membrane also showed antimicrobial effects against all tested bacteria. The presence of curcumin and aspirin in the asymmetric membrane enhanced osteogenic potential at both transcriptional and translational levels. The results of the animal test showed that the test area was completely filled with new bone after just 28 days, while the commercial membrane area remained empty. There was also a soft tissue layer above the new bone area in the test side. We suggested that the prepared membrane in this work could be used as a GBR membrane to keep soft tissue from occupying bone defects in GBR surgeries. Besides, the surgeries can be benefited from antibacterial activities and bone healing effects of this novel GBR membrane while, simultaneously, promoting bone regeneration.

Bone defects are considered among the common devastating problems worldwide. Although bone grafting has been applied in the clinic to solve this issue, it has been reported that the rapid migration of fibroblasts to the defect or fracture site can shape a fibrous capsule which prohibits the efficient growth of blood vessels and osteoblasts into the graft tissue and finally result in bone nonunion¹. New developed guided bone regeneration (GBR) methods which effectively halts bone destroying and improves new bone generation hold promise in this context^{2,3}. Creation and maintenance of a secluded space via a barrier membrane is a fundamental rule in GBR which inhibits invasion of the rapidly growing fibrous capsule and other soft tissues and thus facilitated the inhabitation of host bone-originated osteoblasts in defect niche⁴. High biocompatibility, satisfactory degradation and mechanical specifications in order to produce proper barrier functionalities, space maintenance and clinical handling should be the essential properties of used membranes^{4,5}. Enhancing these properties and the ability to complete new bone regeneration via membrane materials is an important research field in bone regeneration.

Nanotechnology is the use of a substance on an atomic, molecular and supra-molecular scale and nanomedicine deals with the medical implementation of nanotechnology. Nanotechnology-based production of

¹Department of Oral and Maxillofacial Surgery, Faculty of Dentistry, Tabriz University of Medical Sciences, Tabriz, Iran. ²Department of Clinical Sciences, Faculty of Veterinary Medicine, University of Tabriz, Tabriz, Iran. ³Infectious and Tropical Diseases Research Center, Tabriz University of Medical Sciences, Tabriz, Iran. ⁴Dental and Periodontal Research Center, Tabriz University of Medical Sciences, Tabriz, Iran. ⁵Stem Cell Research Center, Tabriz University of Medical Sciences, Tabriz, Iran. ⁶These authors contributed equally: Mohammad Ali Ghavimi and Amirhossein Bani Shahabadi. ✉email: maleki.s.89@gmail.com; sharifi.ghazi@gmail.com

asymmetric membranes is considered to be a perfect bone healing which provides a top layer that acts as an inhibitory barrier against pathogen invasion and physical damages and also an inner layer which allows bone resorption and maintains the niche that is crucial for bone regeneration^{6,7}.

Electro-spinning as a conventional textile industry using polymer science has lately been introduced as a novel strategy in the production of nanoscale biomimetic scaffolds in tissue engineering. It is also a promising controlled drug delivery system which allows the incorporation of therapeutic agents into the non-woven nanofiber meshes during the electrospinning process².

Collagen as the main constituent of skin, bone, tendon, and connective tissue of animals is an appropriate scaffolding material for tissue engineering areas⁸. Owing to its outstanding biocompatibility and biodegradability, collagen membranes have been applied in the GBR technique and have shown suitable clinical outcomes⁹.

Curcumin, the main bioactive constituent of turmeric, has been recognized and revealed to have a remarkably extensive range of useful biological functions such as anti-microbial, anti-cancer, antioxidant, anti-inflammatory, anti-angiogenic activity¹⁰. Moreover, it shows beneficial effects in wound healing processes^{11–13}. Safety assessment evaluations confirmed that curcumin is very safe as it is tolerated high concentrations without any toxic impacts¹⁴. According to reports, curcumin has shown promoting bone healing as well. Besides, the local administration of curcumin containing nanomaterials efficiently prevented bone resorption and inflammation related to experimental periodontal disease^{15,16}.

Aspirin (acetylsalicylic acid) has been broadly applied for years as a non-steroidal anti-inflammatory drug (NSAID). Recently, some reports have shown that aspirin can accelerate bone repair and may control the balance between bone formation and bone resorption and prevent the differentiation and maturity of osteoclasts^{17,18}. It has been reported that aspirin can prevent from invading soft tissue to bone defects in GBR surgeries¹⁹. Several studies have shown the application of some NSAIDs for repairing bone tissue, particularly in bone healing and the treatment of bone fractures²⁰. The study of Cao et al. on mini swine calvarial bone defect model displayed that aspirin causes to accelerate the regeneration of bone marrow mesenchymal stem cells (BMSC). Their study exhibited that aspirin at 75 µg/ml stimulated the osteogenesis of BMSC in vivo and in vitro, displayed by new bone volume in the nude mice transplantation model and alizarin red staining ($p < 0.01$), respectively. Treatment of defects with aspirin-BMSC caused better new bone fill significantly at 6 months' post-surgery ($p < 0.01$). The concentration of IFN- γ and TNF- α was reduced significantly with aspirin-BMSC treatment ($p < 0.05$)²¹.

Generally, directly combined drugs into the GBR membranes, which lead to the fast release of the drugs from the membranes, subsequent in a high burst release and short release period²². Gastric erosion and hemorrhagic micro-bleeding are side effects of aspirin, which resulted from long-term use of it, but topical and low-dose applications of aspirin for therapy of disease would be very hopeful²³.

The aim of the current study was to design an asymmetric membrane including aspirin-loaded PLGA nanoparticles and curcumin nanofibers for guided bone regeneration purposes.

Materials and methods

Materials. The materials used are specified as in the following: 2,2,2-Trifluoroethanol and Glutaraldehyde (25% Aqueous Solution) purchased from Merck (Darmstadt, Germany). Fetal bovine serum (FBS), Dulbecco's modified Eagle's medium (DMEM), Dulbecco's phosphate buffer saline (DPBS), trypsin, penicillin G and streptomycin were achieved from Gibco (Life Technologies, Carlsbad, CA, USA). poly lactic-co-glycolic acid (PLGA (75:25), Acetylsalicylic acid (Aspirin), curcumin, collagen (Bovine type), Dimethylsulfoxide (DMSO), MTT (3-[4,5-dimethyl-thiazol-2-yl]-2,5-diphenyl-tetrazoliumbromide), paraformaldehyde, glycerol phosphate, ascorbic acid, dexamethasone, RIPA buffer, protease inhibitor cocktail, Alkaline Phosphatase Assay Kit, QuantiPro BCA Assay Kit were bought from Sigma-Aldrich (Darmstadt, Germany). Pluronic F68 was obtained from MPBIO (Illkirch Cedex, France), RNA extraction kit was purchased from GeneAll (Seoul, Korea). DNase I was obtained from Thermo Fisher Scientific (Hamburg, Germany). HOT FIREPol EvaGreen (no ROX) qPCR mix kit and cDNA synthesis kit obtained from Solis Biodyne (Tartu, Estonia). Mouse anti-rabbit osteocalcin (OCN), Runx-2 and GAPDH primary antibodies as well as goat anti-rabbit secondary antibody were purchased from Santa Cruz Biotechnology (Santa Cruz, CA, USA). Western Blotting Luminol Reagent and Blotto solution were purchased from Santa Cruz Biotechnology (Santa Cruz, CA, USA). All the primers were purchased from Metabion (Lower Saxony, German). The dental pulp stem cells (DPSCs) were purchased from Dental Research Center, Tehran, Iran. All solvents were acquired at lab-grade purity and utilized without further purification.

Methods. In this work, we prepared an asymmetric GBR membrane. Collagen nanofibers (CNFs) including PLGA-aspirin nanoparticles (PANPs) as was one side of the asymmetric membrane (PACNFs), and curcumin/collagen nanofibers on the other side of the asymmetric membrane (CCNFs).

Production of aspirin-loaded PLGA nanoparticles. In the first step, 100 mg PLGA was dissolved in acetic acid and water. Then, 3 mg of aspirin was added to anhydrous ethanol to produce a saturated solution and then individually added to the PLGA solution under magnetic steering of 100 rpm at 25 °C (solution 1). In a separate beaker, 50 ml pluronic F68 was added into 50 ml dichloromethane under magnetic steering of 100 rpm at 25 °C (solution 2). The solution 1 was then added into solution 2 drop by drop and for 10 min was stirred (450 rpm, 25 °C). The obtained suspension was repeatedly washed with distilled water and then transformed into freeze-dried at (– 55 °C and for 24 h).

Fabrication of asymmetric membrane. Collagen solution in 2,2,2-Trifluoroethanol (8% w/v) was prepared. Passive loading of PANPs (adding the nanoparticles in the polymeric solution prior to electrospinning) was used for the fabrication of PANPs-loaded collagen nanofibers. For this, 10 mg of the prepared PANPs was suspended in 10 ml of collagen solution under constant stirring in dark conditions. Then, the obtained suspen-

sion was electrospun by electrospinning technique (ANSTCo RN/I, Iran). A capillary tube in a vertical form was used. A collector also was used to collect the nanofibers over the electrospinning jets (20 kV voltage, distance of 10 cm between a collector and a capillary tube and 1.5 ml/h flow rate). A white nanofibrous sheet was formed on the collector.

For the preparation of collagen/curcumin side, 5 mg curcumin and 1 g collagen were dissolved in 2,2-Trifluoroethanol. A yellow solution was obtained. In the next step, the yellow solution was electrospun using a similar electrospinning process. The prepared membrane was cut in 1×1.5 cm and was stored for more investigations.

Characterization. The mean size for PANPs and the mean fiber diameter of the nanofibers of the membrane (both sides) was measured by Dynamic Light Scattering (DLS) method (Malvern, United Kingdom) at 25 °C. Furthermore, SEM images (SEM, TESCAN, Warrendale, PA) were acquired to assess the morphology of the PANPs as well as electrospun nanofibers in both side of the membrane. For SEM images, the prepared nanomaterials were fixed via an adhesive tape on aluminum stubs and covered with gold before the examination. Transmission electron microscopy (TEM) was used to confirm the presence of PANPs in the matrix of CNFs ([TEM], JEM-2100F; JEOL, Tokyo, Japan). Enough low electron density was used in order not to melt the polymers or destroy nanofibers structure.

Measurements of the zeta potential were done using a zeta-sizer (Malvern, UK) at 25 °C in order to evaluate the surface charge of the nanomaterials. For this, the suspension of nanomaterials was diluted with water and injected into the capillary cell of zeta-sizer. The qualitative comparison of crystalline state of the components of the material was examined by the X-ray diffraction (XRD) technique (Philips TW 1710 diffractometer with Cu-K α incident radiation regulated at 40 kV and 30 mA). The records were done at room temperature over the 2θ range of 20°–60°, with scanning rate 3°/min. Besides, to get the molecular structure and inter/intra molecular bonding of the prepared nanomaterials, Fourier transform infrared spectroscopy (FTIR) was used (Thermo Scientific FTIR (Thermo Nicolet-6700) spectrophotometer) in the range 4000–400 cm^{-1} .

In vitro release of PANPs from the asymmetric membrane. To assess the release outline of aspirin from the prepared membrane, a small piece of the asymmetric membrane was put under magnetic steering in 300 ml of phosphate buffer medium (100 rpm, pH of 7.4, and temperature of 37 °C). At seven time points (1, 5, 10, 15, 20, 25 and 30 days), 2 ml of the medium was collected and then replaced with the same volume of the primary buffer medium without aspirin. The amount of aspirin was then measured by ultraviolet spectrophotometry at 280 nm ($n=3$) for each point. Aspirin concentration was calculated using a standard curve and the release pattern was illustrated.

Microbial test. Antibacterial effects of the prepared membrane were evaluated by disk diffusion agar on the Muller-Hinton agar against *Staphylococcus aureus* (*S. aureus*), *Escherichia coli* (*E. coli*) and *Enterococcus faecalis* (*E. faecalis*). Briefly, the bacterial cell suspension equivalent to the 0.5 McFarland standard (1.5×10^8 CFU/mL) was inoculated on the Muller-Hinton plates using a swab and allowed to dry for 10 min. Six millimeters disk-shaped membranes were placed on the agar surface and plates were incubated at 35 °C for 24 h aerobically. Collagen nanofibrous membrane (without any potential ingredient) was used as control disk. The inhibition zones around the disk were measured and considered as representing of the antibacterial activity of tested membranes.

Evaluation of biocompatibility; in vitro. The sterilized membranes were cut into discs with a diameter of 0.32 cm^2 to match the 96-well plate size and pre-wetted with the complete culture medium (i.e., DMEM with 10% FBS, 100 mg/mL of streptomycin and 100 U/mL of penicillin), and then the cells were added. Next, we seeded 5000 DPSCs onto the membranes in 200 μL of the medium and incubated the membranes at 37 °C in a 5% CO_2 atmosphere. The wells' original culture medium was replaced at different times after culture (24 h, 72 h, and day 7), with MTT (50 μL /well, i.e., 2 mg/mL) in addition to fresh medium (150 μL /well). Then, the plates were incubated for 4 h at 37 °C in the 5% CO_2 atmosphere. Afterward, we replaced the 200 μL /well of DMSO with the wells supernatant for 30 min. Next, 100 μL of the solution was moved to another 96-well plate and the absorbance was determined at 570 nm using a Microplate Reader.

Cell differentiation. We seeded DPSCs (5000 cells/ cm^2) in 6-well plates on each sterile membrane and allowed them to time for cell adherence on the membranes surface through incubating at 37 °C and 5% CO_2 in basal medium for 24 h. Then, the basal medium was exchanged with osteogenic medium (i.e., the basal medium which is supplemented with 0.2 mM ascorbic acid, 10^{-8} M dexamethasone, and 10 mM β -glycerolphosphate). We refreshed the osteogenic medium every 72 h for 21 days—we cultured DPSCs in the osteogenic medium as control groups.

RNA extraction and cDNA synthesis. On day 21, we extracted the total RNA using an RNA extraction kit following the kit's protocol (GeneAll, Seoul, Korea). To eliminate the genomic DNA, we used DNase I was according to the manufacturer's protocol. Next, the extracted RNAs were normalized based on their RNA content, which was determined by a NanoDrop spectrophotometer (ND-1000, Thermo Fisher Scientific, MA, USA). We used cDNA synthesis kit according to the kit manual for cDNA synthesis, using a LightCycler instrument (Roche Applied Science, USA).

Gene expression. We used a real-time polymerase chain reaction (qRT-PCT) kit to evaluate gene expression. We used the following primers: (housekeeping; 5'-AGCCACATCGCTCAGACAC-3', 5'-GCCCAATAC

GACCAAATCC-3'), OCN (late marker of osteogenesis; 5'-AGCAAAGGTGCAGCCTTTGT-3', 5'-GCGCCTGGGTCTCTTCACT-3'), and RUNX2 (early marker of osteogenic differentiation; 5'-ATCTGAGGTAACCTGCTAACG-3', 5'-CCGAAGTCAACATATCAATACAC-3). The $2^{-\Delta\Delta CT}$ method was applied to calculate the fold change expression of the target genes.

Biochemical assays. At three points on day 7, day 14, and day 21, we drained the osteogenic medium, and to eliminate the serum proteins, we submerged the DPSCs seeded membranes for 8 h in serum-free DMEM, after that, we conducted DPBS washing three times. The lysis buffer (i.e., 10 mM Tris which was supplemented with 0.2% Triton in PBS) was used for DPSCs lysis. This lysate was used to evaluate the activity of ALP employing ALP assay kits.

Western blotting. The RUNX2 and OCN protein expression was quantified, as osteogenic markers using Western blotting at day 21. In short, after serum protein elimination, we lysed the DPSCs-seeded membranes using a RIPA buffer which was supplemented with a protease inhibitor cocktail. We run the lysates with the same level of total protein (as measured using a BCA kit) through 7.5% SDS-PAGE gel. Next, the separated proteins were transferred to a nitrocellulose membrane. We blocked the membranes using 2% non-fat dry milk in 0.1% TBS-T (Tris-buffered saline/Tween-20). Afterward, we incubated the nitrocellulose membranes in primary, and horseradish peroxidase (HRP) conjugated secondary antibodies. Then, we used Clarity Western ECL Substrate (Bio-Rad, USA) to visualize the bands of the membrane. A commercial molecular weight marker (Thermo Scientific, USA) was used to identify the protein bands. The Image J software package was used to determine the density of each band. Also, the relative density of the target proteins was normalized to GAPDH.

In vivo bone regeneration behavior. To study the bone regeneration performance of the prepared membrane, a model of alveolar bone defect using 6 adult mongrel dogs were performed. Dogs were anesthetized by intramuscular injection of 10 mg/kg ketamine 10%, 0.1 mg/kg acepromazine 2% and Cocktail IM. A defect was generated (8 mm in diameter and 4 mm deep) on both sides of the dogs' jaw with a 6 mm trephine drill, which was cooled while washing with sterile saline. One side as test side for insertion of the prepared membrane (15 mm in diameter) and the other side as control side. In the control side, the defects were covered with the commercial membrane (Regen collagen, 15 mm in diameter). The periosteum and skin were sutured using 5-0 monofilament vicryl suture in an interrupted fashion.

On day 28, we anesthetized the dogs for surgery. The samples were immobilized in a hydrochloric acid solution of formaldehyde. Then, we decalcified them in 17% EDTA solution and dehydrated them using an ascending graded alcohol series. Lastly, we fixed them in paraffin. A series of cross-sections with a diameter of 5 μ m in the center of bone defects were prepared. Then, we made them by hematoxylin and eosin (H&E) staining for investigation under light microscopy (BX51, Olympus, Japan). The institutional ethics committee of the Tabriz University of Medical Sciences agreed with the use of animals for the experiments conducted in this study, and all experimentations were done based on the related guidelines and rules.

Statistical analysis. All data were stated as the mean \pm standard deviation. To show statistical significance, $p < 0.05$ was considered.

Ethical considerations. The institutional ethics committee of the Tabriz University of Medical Sciences agreed with both theses and all experimentations were done based on the related guidelines and rules. The code of ethics for preparation and physicochemical assessments was IR.TBZMED.REC.1397.317. For cellular and in vivo investigations the code of ethics was IR.TBZMED.VCR.REC.1399.164.

Results and discussions

Electrospinning set up. The shape and the size of the nanomaterials should be well-ordered, which is not a simple procedure. The growing of particles from atoms to nanometric or micrometric sizes can be managed to yield mono-dispersed sizes^{6,24}. Electro-spinning as a quickly developing technique displays the ability to form varied morphologies due to its functionality, flexibility, and simplicity. Processing variables for the electrospinning process including needle to collector distance, voltage, flow rate, also, solution parameters such as surface tension, viscosity, and electrical conductivity of the solution can control the morphology of the nanofibers⁸. The goal of electrospinning procedure optimization is to identify the conditions of producing fibers with a minimum diameter²⁵. Optimum settings in our study were: 20 kV voltage, distance of 10 cm between a collector, a capillary tube 1.5 ml/h flow rate. In this study, we used the passive loading of PANPs into collagen nanofibers (adding the nanoparticles in the polymeric solution prior to electrospinning). The results of other investigators showed that polymeric nanoparticles, nanotubes, micelles, lipid nanoparticles and etc. can be embedded with electrospun nanofibers to improve different parameters like release outline, drug safety, drug-loading efficiency, and better functionality of the fibers^{26–29}. Nanofibers embedded with nanoparticles are similar to co-axial nanofibers as they keep drug safe from organic solvents in the production period and extend the period of drug delivery³⁰. Furthermore, it is a more simple technique than co-axial electrospinning because it applies a single nozzle. Figure 1 shows the pictures for the prepared membrane.

Physicochemical properties. To assure from the prepared nanocarriers suitability for different uses, they should be characterized. The important physicochemical properties of nanomaterials are the mean particle size and point diffraction interferometer (PDI), which affect the endocytosis-dependent cellular uptake³¹. The mean

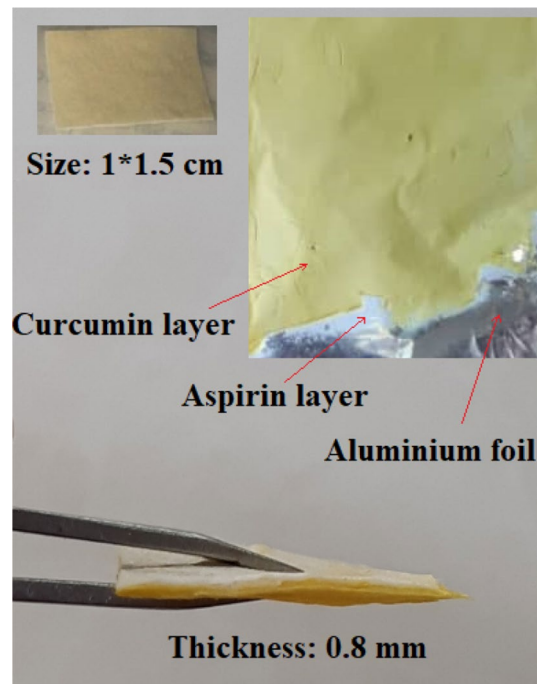


Figure 1. The pictures for the prepared membrane.

diameter of nanofibers is a main and key parameter that can influence on different properties of nanomaterials in biomedical uses. With respect to the particle size distribution, PDI values more than 0.7 shows that the nanomaterial has a very wide distribution of particle size and is maybe unsuitable to be analyzed by DLS method³². The size distribution of the prepared nanomaterials is presented in Fig. 2. The results obtained from DLS showed a mean size of 50.44 nm (PDI of 0.28) for PANPs, 98.52 nm (PDI of 0.49) for PACNFs and 84.06 nm (PDI of 0.39) for CCNFs. The obtained results display the production of relatively mono-dispersed nanomaterials.

SEM results displayed uniform agglomerated spherical morphology for PANPs (Fig. 3A). For the prepared nanofibrous asymmetric membrane, SEM results showed successfully formation of nanofibers (Fig. 3B, C). It can be noticed from the SEM results that the nanofibers were randomly electrospun on the collector with high similarity to the construction of the ECM. Furthermore, the nanofibers displayed a network-shaped construction without the presence of beads. Biomimetic nanofibrous scaffolds simulate important properties of the natural ECM, so offer a desirable approach to restore functions or attain desirable responses for tissue regeneration. By modifying the electrospinning parameters controllable fibrous structures can be successfully produced and so offer excellent prospects for the production of biomimetic materials^{33,34}.

The anisotropic architecture of natural ECMs is critical for tissue function³⁵. Hence, a well-defined architecture is essential for accurately imitate natural ECM for tissue regeneration or guiding cell growth^{36,37}. For this purpose, electrospun nanofiber scaffolds with numerous alignments such as radially aligned, yarn, axially aligned have displayed excellent capability in guiding cell migration, shaping cell morphology, and affecting cell differentiation compared with the other kinds of scaffolds both in vivo and in vitro^{38–40}. More significantly, specific cellular activities such as cell differentiation, adhesion and migration may lead to promising adaptation of cells in this fibrous membrane as nanoscale microenvironment⁴¹.

SEM images sometimes does not show the existence of nanoparticles in the matrix of another polymer. Then, it should be checked using TEM. TEM image (Fig. 3D) showed the presence of PANPs in the matrix of nanofibrous asymmetric membrane. As it can be observed, PANPs deposited as spherical entities along the nanofibers. In TEM, the image formation is related to the scattering of electrons by materials of differing density. The higher the density, the darker the TEM image and the lower the density, the brighter the image⁴². Then, due to the higher density of PLGA (75:25) than collagen, the PANPs are darker in TEM image.

Zeta potential measurements (Fig. 4) showed a negative surface charge for all nanomaterials (-25.92 mV for PANPs (Fig. 4a), -32.20 mV for CCNFs (Fig. 4b) and -37.74 mV for CNFs (Fig. 4c)). The surface charge of the particles has main role on their properties. Zeta potential is one of the key parameters usually utilized to estimate suspension stability. As a general rule in stability reports, a value of zeta potential above ± 60 mV shows outstanding stability, while zeta potential less than ± 5 mV generally consequences in particle aggregation. The values between this range results good stability or satisfactory short-term stability. It shows the repulsive charge between the fibers is enough to evade agglomeration^{43,44}. Then, the prepared nanomaterials indicated good stability. It has also been informed that the negative zeta potential shows a significant promising impact on the attachment and proliferation of the bone cells. The reports showed that a surface with a negative charge is more available for the attachment and proliferation of osteoblasts than neutral or positive charges^{45–47}.

The X-ray diffraction (XRD) method of the fabricated nanomaterials were measured to confirm the production of the materials and for the qualitative comparison of crystalline state of the constituents of the material. The

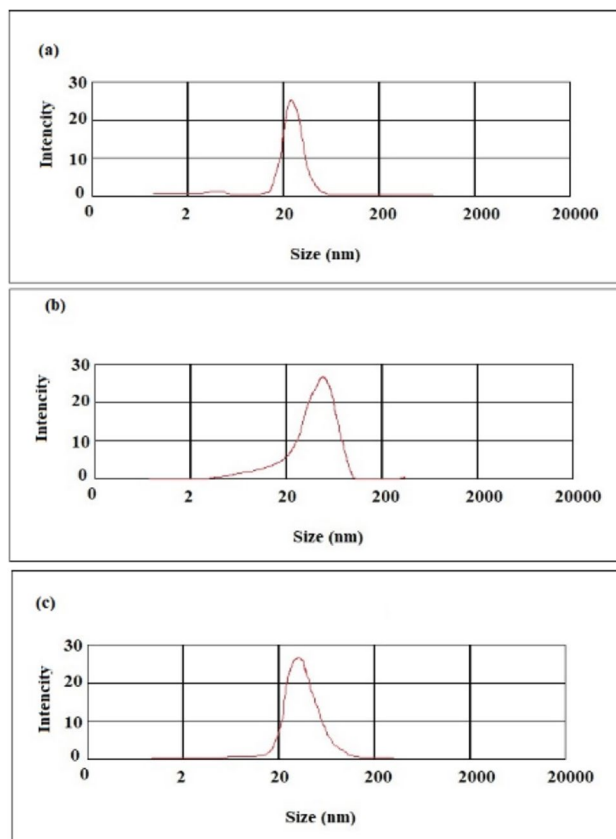


Figure 2. Size distribution of the prepared membrane: (a) aspirin-loaded PLGA nanoparticles, (b) nanofibrous asymmetric membrane (CCNFs side), (c) nanofibrous asymmetric membrane (PACNFs side).

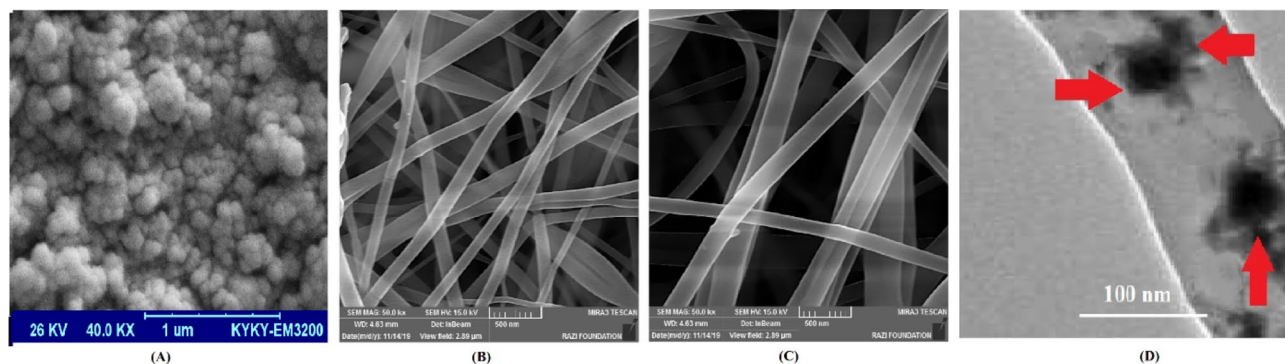


Figure 3. Microscopic images of the prepared membrane: (A); aspirin-loaded PLGA nanoparticles, (B); the asymmetric membrane (CCNFs side), (C); the asymmetric membrane (PACNFs side), (D); TEM image of the presence of PANPs in the matrix of the CNFs side.

results for the XRD pattern displays the existence of sharp and high intensity peaks for the prepared aspirin-loaded PLGA nanoparticles as well as the asymmetric nanofibrous membrane (Fig. 5A). The appearance of diffraction two-theta (2θ) peaks at 7° , 15° , 20° , 22° and 27° , corresponding to the characteristic crystal form of aspirin as reported in the literature⁴⁸. Aspirin-loaded PLGA nanoparticles showed all characteristic peaks of aspirin but appear less intense as compared to pure aspirin⁴⁸ which is due to the amorphous nature of the PLGA^{49,50}. The XRD pattern of curcumin displayed sharp and intense peaks between 10° and 30° , representing a crystalline arrangement. The major XRD diffraction peaks of curcumin were detected at angles of 9° , 14° , 17° , 18° , 21° , 23° , 24° and 25° ^{51,52}. The XRD diffractogram of the membrane displayed a typical amorphous peak at 20° , which implied that neither collagen nor PLGA could not be crystallized in the course of electrospinning and gave an amorphous structure in the nanofibers. The membrane also showed a reduction in the number of peak intensity for curcumin and aspirin-loaded PLGA nanoparticles (as compared to their pure peak), indicating decreased crystallinity or changes into the amorphous phase of the material during the electrospinning

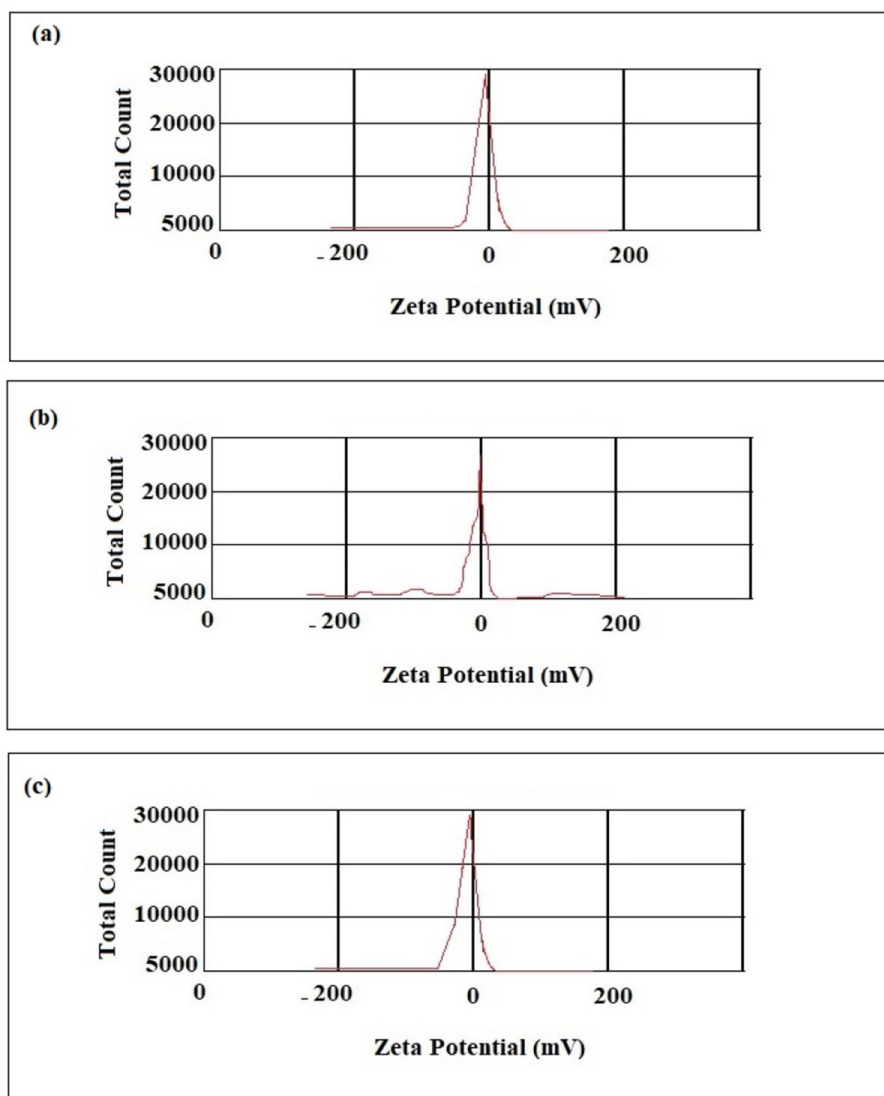


Figure 4. Zeta potential of the prepared materials; (a) aspirin-loaded PLGA nanoparticles (PANPs), (b) nanofibrous asymmetric membrane (CCNFs side), (c) nanofibrous asymmetric membrane (PACNFs side).

process^{9,53}. The obtained outcomes are similar to the earlier study on the collagen–chitosan fibers that according to the authors it could be due to the cooperative effect of the solvent and electrospinning procedure on the chitosan and the collagen⁵⁴.

To evaluate the molecular structure of the prepared nanomaterials, FT-IR was applied. FT-IR peaks (Fig. 5B) showed all characteristic peaks of the prepared nanomaterials with no additional peaks. Four characteristic absorption peaks at 1680 (carbonyl group), 1608 (benzene ring) and a broad peak in the range 2500–3500 cm^{-1} (carboxylic acid group) were observed in the aspirin sample and were also present in the aspirin-loaded PLGA nanoparticles as well as membrane confirming the presence of aspirin-loaded PLGA nanoparticles within asymmetric membrane^{55,56}. The spectrum of PLGA showed the C=O absorption band at 1760 cm^{-1} which was also seen in aspirin-loaded PLGA nanoparticles as well as asymmetric membrane^{52,57}. Curcumin showed the characteristic intensities of O–H stretching at 3450 cm^{-1} , the aromatic C=C stretching at 1580 and 1480 cm^{-1} , C=O stretching at 1600 cm^{-1} , aromatic C–O stretching at 1250 cm^{-1} , aliphatic C–O stretching at 1180 cm^{-1} and =C–H bending at 980 and 900 cm^{-1} . C=O stretching appeared at low frequency due to enolization and intermolecular H-bonding⁵². In the FTIR pick of collagen, the main functional groups of collagen were detected. The main peaks were amide I (1680–1620 cm^{-1}), amide II (1580–1480 cm^{-1}), and amide III (1300–1200 cm^{-1}). The strong hydroxyl band in the region of 3200–3600 cm^{-1} was observed to be overlapped with the amide A band (3360–3320 cm^{-1})⁵⁸.

The release of aspirin in vitro. An aspirin-loaded nanoparticle has been produced and applied to determine that aspirin can be released in a sustained form in vitro (Fig. 6). The calibration curves of the absorbance of aspirin at 280 nm displayed an $R^2=0.996$. A burst release of aspirin was obtained for first to fifth days followed by a sustained release until day 30.

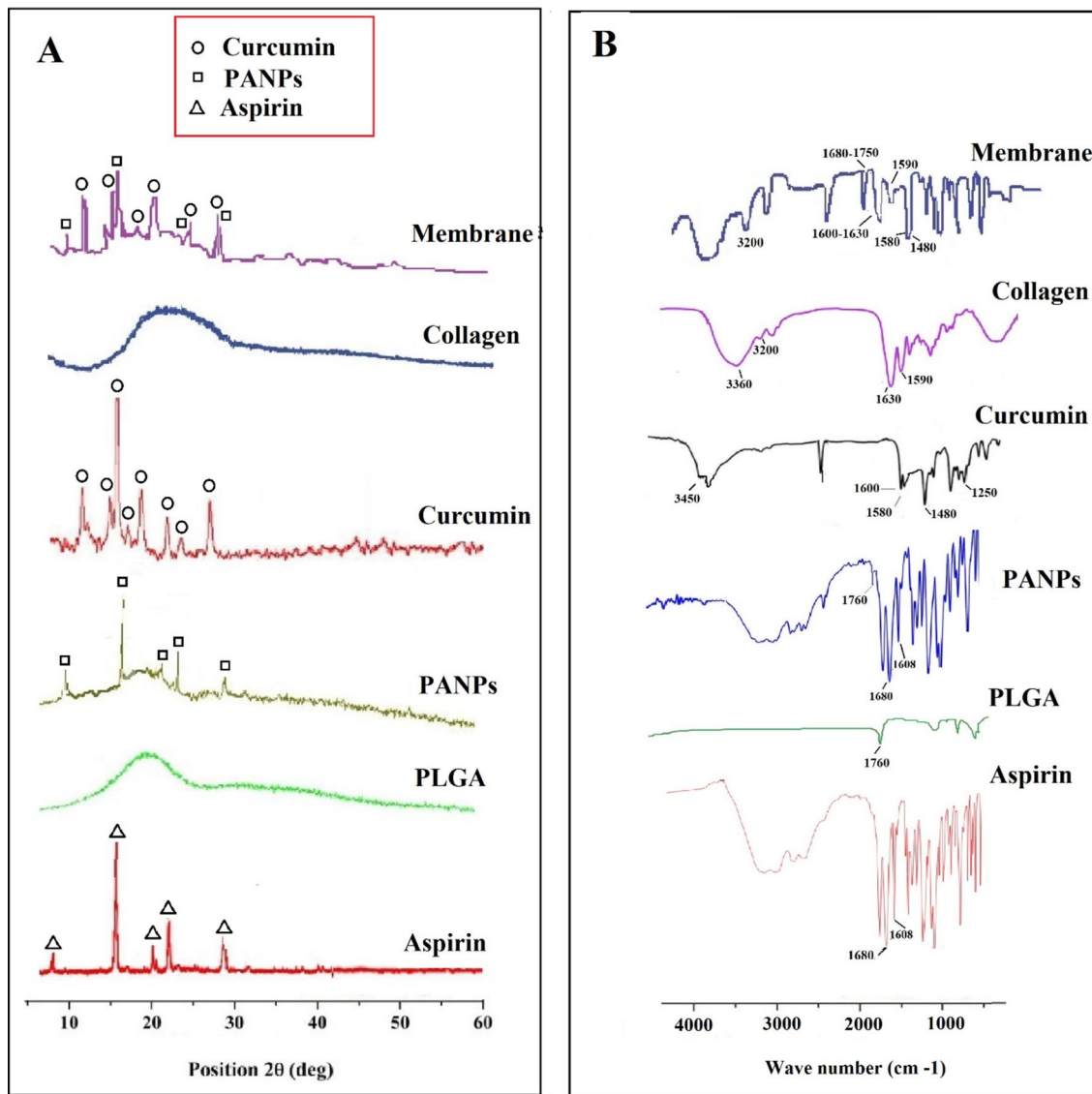


Figure 5. X-ray diffraction pattern (A) and FTIR patterns (B) for; aspirin, PLGA, aspirin-loaded PLGA nanoparticles, curcumin, collagen and asymmetric membrane.

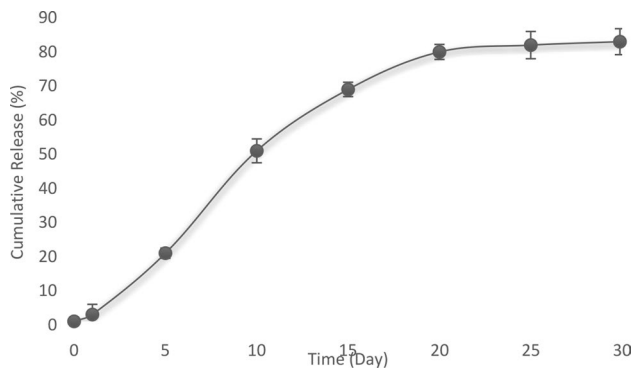


Figure 6. Release curve of aspirin from the asymmetric membrane at 1, 5, 10, 15, 25 and 30 days.

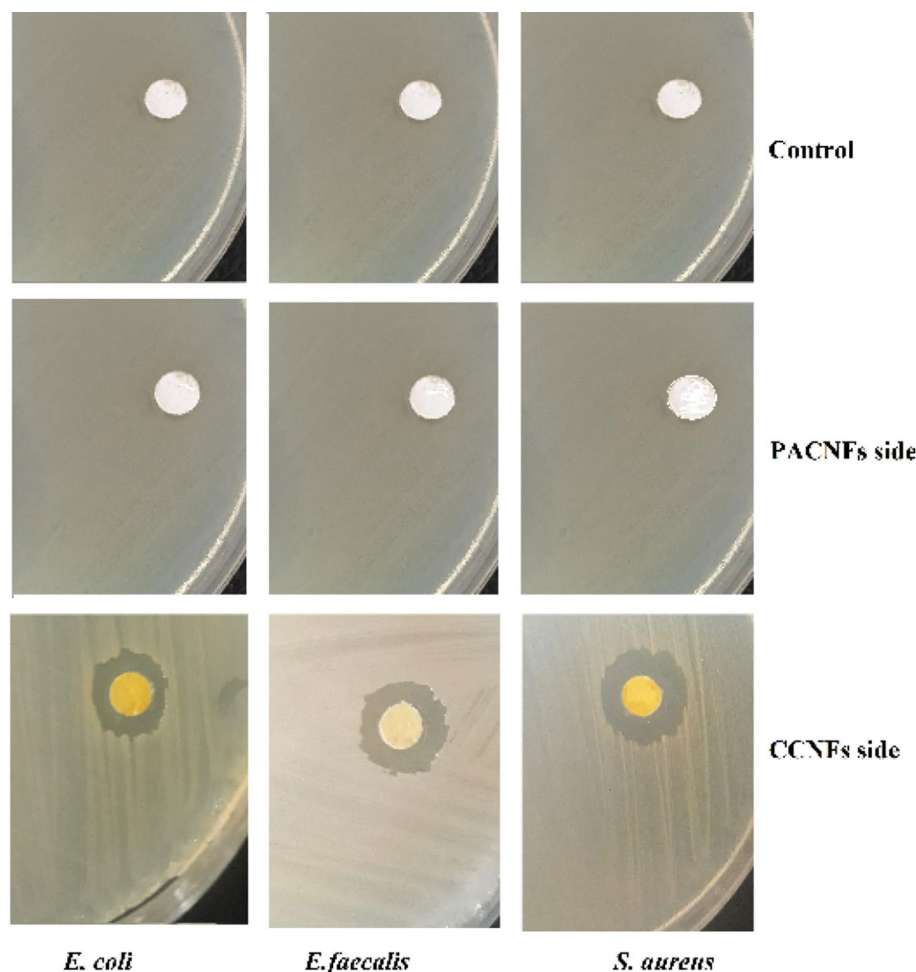


Figure 7. The antibacterial effects of the membrane against *S. aureus*, *E. faecalis* and *E. coli* by detecting the growth inhibition of bacterial isolates around the membrane disks.

Diffusion and polymer degradation are two main mechanisms of drug release from the polymer matrix⁵⁹. According to Fig. 6, aspirin showed a controlled release profile from the asymmetric membrane. Then, the aspirin not only diffuses through PLGA nanoparticles, but also through the collagen membrane. The initial release concentration of aspirin from the asymmetric membranes was higher (20% for first to fifth days), which was due to the drug diffusion from the surface of the nanoparticles and subsequently from the surface of the asymmetric membrane. Furthermore, late in the release profile, the aspirin concentration was lower but aspirin has sustained-release until the 30th day. It can be suggested that the release may be because of both the diffusion of aspirin from the surfaces of the nanoparticles and the asymmetric membrane and the degradation the matrix of the asymmetric membrane⁵⁹.

Microbial test. The antibacterial effects of the membrane was evaluated against *S. aureus*, *E. faecalis* and *E. coli* by detecting the growth inhibition of bacterial isolates around the membrane disks. The membrane was more effective against *S. aureus* followed by *E. faecalis* and *E. coli* (Fig. 7). The antimicrobial effects of nanocurcumin have been reported against both Gram-negative and Gram-positive bacteria⁶⁰. However, it is reported that the nanocurcumin is more effective against Gram-positive bacteria than Gram-negatives bacteria^{61,62}. There was not an observable inhibition zone around the disk of PACNFs side as well as control disk.

Cellular studies. *The DPSCs proliferation.* The results of the DPSCs proliferation or metabolic activity (Fig. 8) shown that the cells were metabolically active on PACNFs and CCNFs membranes. Throughout the 72 h and 7 days of culturing DPSCs. The metabolic activity (proliferation) of DPSCs on PACNFs membrane was found to be higher than CCNFs membrane. This increase in proliferation of DPSCs can be partially related to the proliferative effect of aspirin and curcumin in PACNFs and CCNFs membranes, respectively^{19,63,64} (Fig. 8).

Osteogenic differentiation. ALP activities of DPSCs seeded on the membranes followed its common trend in osteogenesis⁶⁵ (an increase from day 7 to 14 related to osteogenic differentiation followed by a reduction

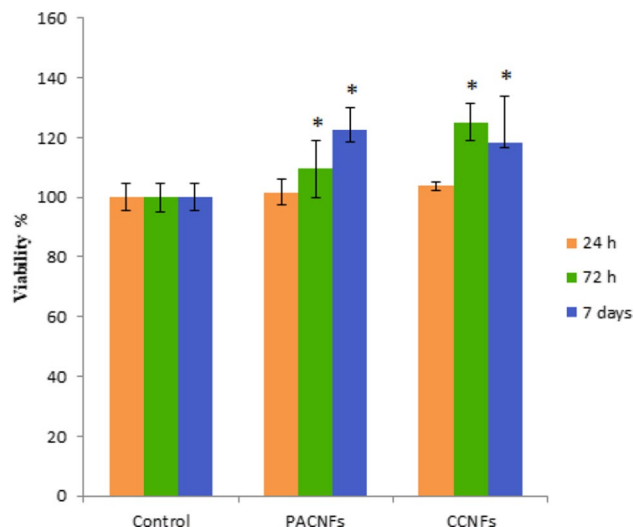


Figure 8. Proliferation of DPSCs cultured on PACNFs and CCNFs membranes at 1, 3, 7 days. An asterisk represents a statistically significant difference ($p < 0.05$) between the test and control group at each time point.

from day 14 to 21 related to the initiation of the mineralization procedure (Fig. 9a). The normalized amount of ALP activity, which has a main role in mineralization, increased in both PACNFs and CCNFs membranes. An increase in the ALP activity of mesenchymal stem cells in the presence of aspirin and curcumin has also been reported in the previous studies^{66,67}.

PACNFs membrane can upregulate Runx-2 and OCN, as osteogenic genes, according to their expression (Fig. 9b, c). Results demonstrated that the aspirin and curcumin significantly affected the DPSCs differentiation ($p < 0.05$). Based on the statistical analysis, there is a significant increase ($p < 0.05$) for the expression of OCN and Runx-2 genes at day 21. The western blot analysis of Runx-2 and OCN proteins on day 21 (Fig. 9d, f) confirm the PACNFs significantly higher osteogenic potential in the stimulation of osteogenic differentiation at the level of translation in DPSCs (see also Supplementary Information). Thus, it may be stated that aspirin and curcumin can both translationally and transcriptionally improve the osteogenic differentiation potential in PACNFs and CCNFs fibers. Aspirin-loaded chitosan nanoparticles (ACS) were prepared by Zhang et al., which was contained in an asymmetric collagen-chitosan membrane (CCM). They demonstrated that the ACS-CCM has a higher osteogenic potential due to sustained aspirin release¹⁹.

Expression of Runx-2 genes which is involved in bone formation and osteoblastic differentiation^{68–70}, and OCN gene which is engaged in the mineralization of bone and terminal osteoblastic differentiation^{71,72}, were assessed in addition to the expression Runx-2 and OCN proteins to investigate the osteogenic differentiation potential of CCNFs and PACNFs membranes.

The Runx-2 gene expression was elevated for both membranes, which may be attributed to the early stages of DPSCs osteogenic differentiation⁶⁸. The elevated OCN expression, which is the most abundant non-collagenous protein in bone ECM, on day 21, may be attributed to the observed profile of Runx-2 gene, because Runx-2 may directly induce the OCN gene transcription⁷⁰. Note that OCN upregulation is critical for the mineralization and terminal osteogenic differentiation⁷¹. Also, the expression of OCN and RUNX-2 proteins (Fig. 9d, f) may elucidate the enhanced mineralization on CCNFs and PACNFs membranes.

The profile of gene expression of the DPSCs, which were seeded on the membranes control group in the osteogenic media, was consistent with the results of other studies^{73,74}. Our findings showed that the new membranes enhanced the osteogenic properties of the collagenic membranes. Increased expression of the osteoblastic genes and associated proteins, besides ALP activity, shows that aspirin and curcumin may enhance the osteogenic differentiation of DPSCs on PACNFs and CCNFs electrospun fibers. In vivo findings of the present study also proved that more significant bone formation on the membranes (Fig. 10).

In vivo bone regeneration behavior. The results of the animal test showed that the test area (the prepared asymmetric membrane) was completely filled with new bone after just 28 days, while the commercial membrane area remains empty. There was also a soft tissue layer above the new bone area in the test side. No significant inflammatory was detected in the pathology specimens, and the membranes were completely degraded. The results of the histological test (Fig. 10) showed that in the prepared membrane area new bone formation can be seen. In the commercial membrane area, the edges of the defect are still sharp and intact, and in the pathology specimen, the dog's previous bone can be seen. The newly created bone was observed in the test membrane in HE staining images together the obtained cellular results, suggesting that the PACNFs layer of the membrane acts as osteoinductive material. The CCNFs layer not only can act as a physical barrier for the GBR technique, but also it also has osteoconductive effects (according to cellular results) that improves the PACNFs layer's action. Besides, the CCNFs layer helps the formation of the soft tissue above the new bone that can be due to wound healing effects

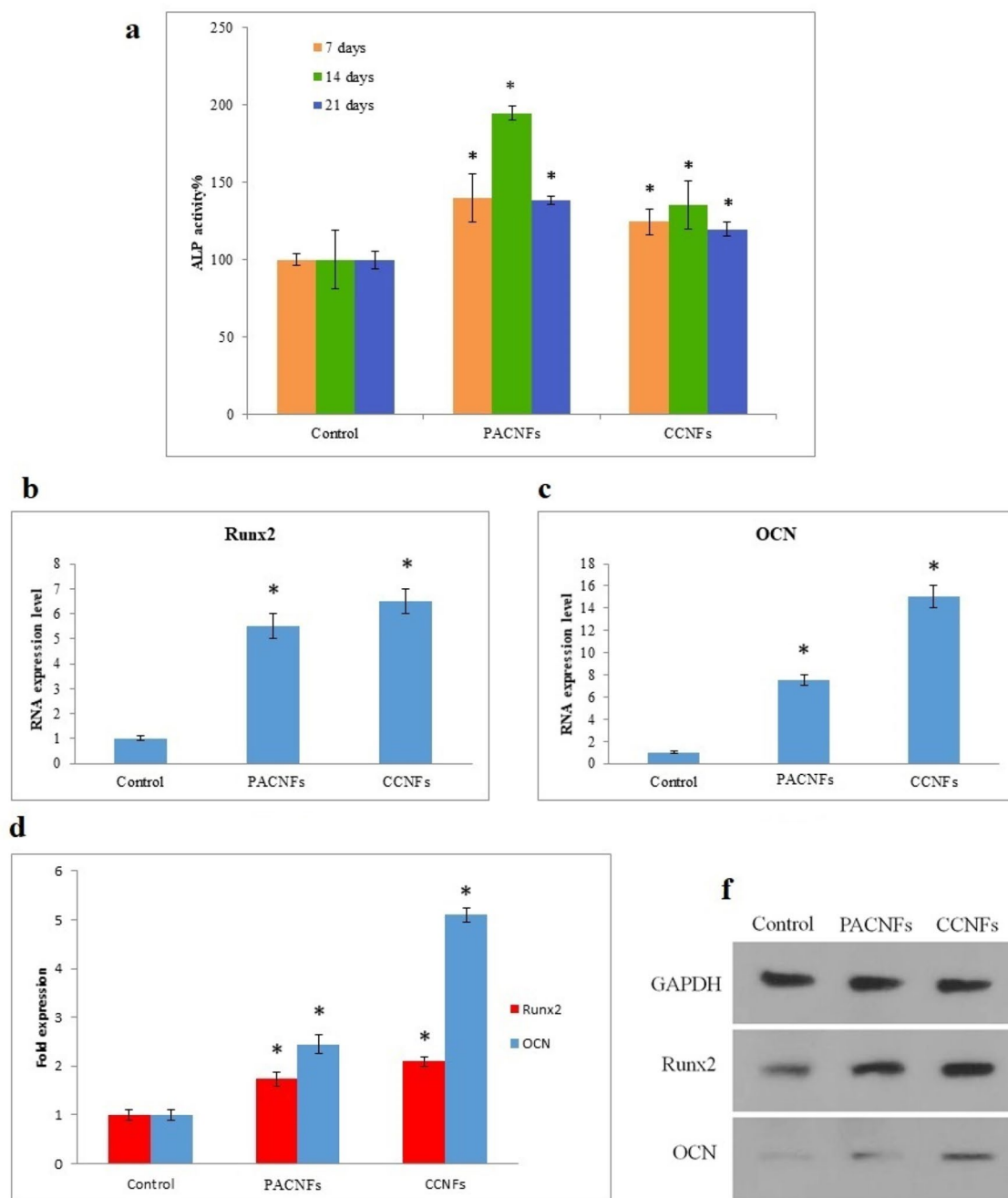


Figure 9. Osteogenic differentiation of DPSCs cultured on CCNFs and PACNFs membranes at days 7, 14, and 21 in the osteogenic medium: activity of ALP (a); expression of genes [Runx-2 (b), and OCN (c)]; expression of proteins OCN and Runx-2 at day 21 compared to the expression of GAPDH (d); bands of western blotting for OCN (6 kDa), Runx-2 (55 kDa), and GAPDH (37 kDa) (e). We used three different gels to visualize the expression of OCN, Runx-2, and GAPDH proteins relative to each other (while keeping similar exposure parameters and acquisition settings). An asterisk shows a significant difference ($p < 0.05$) between the control and test groups.

of curcumin. Furthermore, the CCNFs side can be used as a local antimicrobial delivery system for avoiding infections in the test surgical area (based on the antimicrobial test results).

The main characteristics and the findings for the prepared membrane were summarized in Table 1.

Conclusion

The main purpose of this study was to design an asymmetric GBR membrane using electrospinning technique for the sustained release and local delivery of aspirin and curcumin. We hypothesized that the prepared membrane in this work acts as osteoinductive material to promote the new bone formation. Besides, the prepared

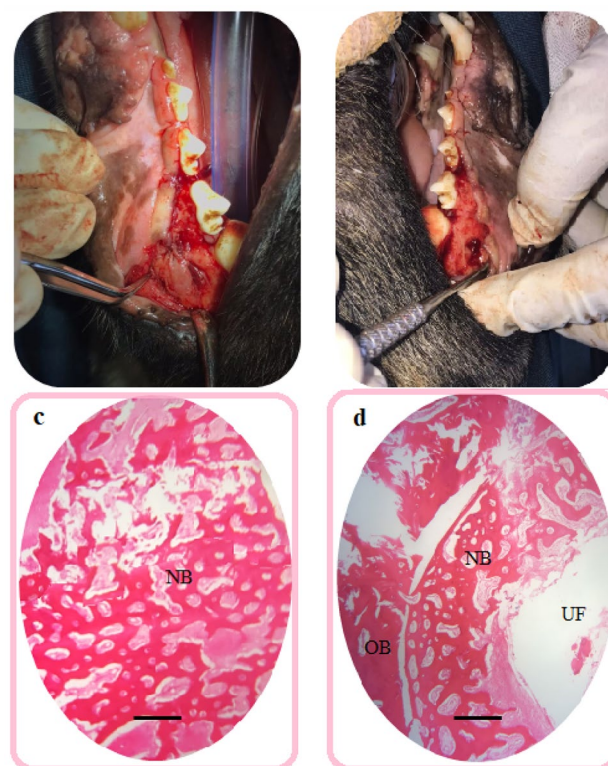


Figure 10. (a) the test area (covered with the prepared asymmetric membrane) that was completely filled with new bone, (b) the control side (covered with the commercial membrane) that remains empty, (c) histological section of bone defects in the test area, (d) histological section of bone defects in the control area; *UF* unfilled area, *NB* new bone, *OB* old bone. Original magnification is $\times 40$. Scale bars = 500 μm .

Main finding of tests	Collagen nanofibers (CNFs) including PANPs (PACNFs)	curcumin/collagen nanofibers (CCNFs)
<i>The asymmetric membrane</i>		
Physical state	White sheet (thickness of 0.4 mm)	Yellow sheet (thickness of 0.4 mm)
The mean particle size and the surface charge	98.52 nm (PDI of 0.49)	84.06 nm (PDI of 0.39)
	With a negative surface charge of -32.20 mV	With a negative surface charge of -37.74 mV
SEM results for morphology	Nanofibers with a network structure and without the presence of beads	Nanofibers with a network structure and without the presence of beads
In vitro cellular examinations	Without any toxic effect on DPSCs	Without any toxic effect on DPSCs
	Increase in proliferation of DPSCs ($p < 0.05$)	Increase in proliferation of DPSCs ($p < 0.05$)
	Increased in ALP activity ($p < 0.05$)	Increased in ALP activity ($p < 0.05$)
	Increase in RNA expression of Runx-2, and OCN as osteogenic genes ($p < 0.05$)	Increase in RNA expression of Runx-2, and OCN as osteogenic genes ($p < 0.05$)
	Increase in protein expression of Runx-2, and OCN as osteogenic genes ($p < 0.05$)	Increase in protein expression of Runx-2, and OCN as osteogenic genes ($p < 0.05$)
Microbial test	Not showed any antimicrobial effects	It showed antibacterial effects against <i>S. aureus</i> , <i>E. faecalis</i> and <i>E. coli</i>
		The membrane was more effective against <i>S. aureus</i> followed by <i>E. faecalis</i> and <i>E. coli</i>
In vivo findings	The asymmetric membrane completely occupied after just 28 days, while the commercial membrane area remains empty	
	No significant inflammatory was detected in the pathology specimens, and the membranes were completely degraded	
	The results of the microscopic examination showed that in the prepared membrane area new bone formation can be seen. The newly created bone was detected in the test membrane in HE staining images, suggesting that the PACNFs layer of the membrane is osteoinductive and that the CCNFs layer not only can act as a physical barrier for the GBR technique, but also it also has osteoconductive effects (according to cellular results) that improves the PACNFs layer's action	

Table 1. The main characteristics and the findings for the prepared membrane.

multipurpose asymmetric membrane not only can keep soft tissue from occupying bone defects in GBR surgeries, but also it benefits from antibacterial activities and bone healing effects of curcumin. In the field of periodontal therapies, bone regeneration remains a more challenging issue. Nano-dentistry is trying its best to apply new signs of progress in tissue engineering and dental practice. With the growth of advanced investigations and deeper understanding of electrospinning sets-ups, it is probable to attain future "smart bone healing devices" proficient in treating all features of bone defects for real clinical uses.

Data availability

The raw/processed data needed to reproduce these outcomes cannot be shared at this time as the data also are part of an ongoing study.

Received: 7 April 2020; Accepted: 15 October 2020

Published online: 23 October 2020

References

1. Urist, M. R. & Mclean, F. C. Recent advances in physiology of bone: Part I. *JBSJ* **45**, 1305–1313 (1963).
2. Lee, Y. J. *et al.* Electrospun fibers immobilized with bone forming peptide-1 derived from BMP7 for guided bone regeneration. *Biomaterials* **34**, 5059–5069 (2013).
3. Van Leeuwen, A. *et al.* Guided bone regeneration in rat mandibular defects using resorbable poly (trimethylene carbonate) barrier membranes. *Acta Biomater.* **8**, 1422–1429 (2012).
4. Gentile, P., Chiono, V., Tonda-Turo, C., Ferreira, A. M. & Ciardelli, G. Polymeric membranes for guided bone regeneration. *Bio-technol. J.* **6**, 1187–1197 (2011).
5. Bottino, M. C. *et al.* Recent advances in the development of GTR/GBR membranes for periodontal regeneration—A materials perspective. *Dent. Mater.* **28**, 703–721 (2012).
6. Dizaj, S. M., Lotfipour, F., Barzegar-Jalali, M., Zarrintan, M.-H. & Adibkia, K. Physicochemical characterization and antimicrobial evaluation of gentamicin-loaded CaCO₃ nanoparticles prepared via microemulsion method. *J. Drug Deliv. Sci. Technol.* **35**, 16–23 (2016).
7. Yazdani, J., Ahmadian, E., Sharifi, S., Shahi, S. & Dizaj, S. M. A short view on nanohydroxyapatite as coating of dental implants. *Biomed. Pharmacother.* **105**, 553–557 (2018).
8. current state and perspectives. Maleki Dizaj, S., Sharifi, S. & Jahangiri, A. Electrospun nanofibers as versatile platform in antimicrobial delivery. *Pharm. Dev. Technol.* **24**, 1187–1199 (2019).
9. Chen, Z., Wang, P., Wei, B., Mo, X. & Cui, F. Electrospun collagen–chitosan nanofiber: A biomimetic extracellular matrix for endothelial cell and smooth muscle cell. *Acta Biomater.* **6**, 372–382 (2010).
10. Sharifi, S. *et al.* Anti-microbial activity of curcumin nanoformulations: New trends and future perspectives. *Phytother. Res.* **34**, 1926–1946 (2020).
11. Abbas, M. *et al.* Wound healing potential of curcumin cross-linked chitosan/polyvinyl alcohol. *Int. J. Biol. Macromol.* **140**, 871–876 (2019).
12. Fereydouni, N. *et al.* Curcumin nanofibers for the purpose of wound healing. *J. Cell. Physiol.* **234**, 5537–5554 (2019).
13. Shefa, A. A. *et al.* Curcumin incorporation into an oxidized cellulose nanofiber-polyvinyl alcohol hydrogel system promotes wound healing. *Mater. Des.* **186**, 108313 (2020).
14. Urakami, K. *et al.* Compositional analysis of copoly (DL-lactic/glycolic acid)(PLGA) by pyrolysis-gas chromatography/mass spectrometry combined with one-step thermally assisted hydrolysis and methylation in the presence of tetramethylammonium hydroxide. *Chem. Pharm. Bull.* **49**, 203–205 (2001).
15. Zambrano, L. M. *et al.* Local administration of curcumin-loaded nanoparticles effectively inhibits inflammation and bone resorption associated with experimental periodontal disease. *Sci. Rep.* **8**, 1–11 (2018).
16. Li, G., Chen, L. & Chen, K. Curcumin promotes femoral fracture healing in a rat model by activation of autophagy. *Med. Sci. Monit.* **24**, 4064 (2018).
17. Tang, J. *et al.* Aspirin treatment improved mesenchymal stem cell immunomodulatory properties via the 15d-PGJ2/PPAR γ /TGF- β 1 pathway. *Stem Cells Dev.* **23**, 2093–2103 (2014).
18. Lee, B.-S. *et al.* Controlled-release of tetracycline and lovastatin by poly (D, L-lactide-co-glycolide acid)-chitosan nanoparticles enhances periodontal regeneration in dogs. *Int. J. Nanomed.* **11**, 285 (2016).
19. Zhang, J. *et al.* Guided bone regeneration with asymmetric collagen-chitosan membranes containing aspirin-loaded chitosan nanoparticles. *Int. J. Nanomed.* **12**, 8855 (2017).
20. Wei, J.-S. *et al.* Effects of aspirin on fracture healing in OPF rats. *Asian Pac. J. Trop. Med.* **7**, 801–805 (2014).
21. Cao, Y. *et al.* Aspirin promotes bone marrow mesenchymal stem cell-based calvarial bone regeneration in mini swine. *Stem Cell Res. Ther.* **6**, 210 (2015).
22. Slots, J. & Ting, M. Systemic antibiotics in the treatment of periodontal disease. *Periodontology* **2000**(28), 106–176 (2002).
23. Ingelfinger, F. (Mass Medical Soc, 1974).
24. Saedi, M., Eslamifard, M., Khezri, K. & Dizaj, S. M. Applications of nanotechnology in drug delivery to the central nervous system. *Biomed. Pharmacother.* **111**, 666–675 (2019).
25. Ghavimi, M. *et al.* Preparation and study of starch/collagen/polycaprolactone nanofiber scaffolds for bone tissue engineering using electrospinning technique. *Eur. Chem. Commun.* **2**, 122–127 (2020).
26. Son, Y. J. & Yoo, H. S. Dexamethasone-incorporated nanofibrous meshes for antiproliferation of smooth muscle cells: Thermally induced drug-loading strategy. *J. Biomed. Mater. Res. A* **100**, 2678–2685 (2012).
27. Ji, L., Saquing, C., Khan, S. A. & Zhang, X. Preparation and characterization of silica nanoparticulate–polyacrylonitrile composite and porous nanofibers. *Nanotechnology* **19**, 085605 (2008).
28. Ionescu, L. C., Lee, G. C., Sennett, B. J., Burdick, J. A. & Mauck, R. L. An anisotropic nanofiber/microsphere composite with controlled release of biomolecules for fibrous tissue engineering. *Biomaterials* **31**, 4113–4120 (2010).
29. Shao, S. *et al.* Controlled green tea polyphenols release from electrospun PCL/MWCNTs composite nanofibers. *Int. J. Pharm.* **421**, 310–320 (2011).
30. Yayon, A., Klagsbrun, M., Esko, J. D., Leder, P. & Ornitz, D. M. Cell surface, heparin-like molecules are required for binding of basic fibroblast growth factor to its high affinity receptor. *Cell* **64**, 841–848 (1991).
31. Gattoo, M. A. *et al.* Physicochemical properties of nanomaterials: Implication in associated toxic manifestations. *BioMed Res. Int.* **2014**, 1–6 (2014).
32. Danaei, M. *et al.* Impact of particle size and polydispersity index on the clinical applications of lipidic nanocarrier systems. *Pharmaceutics* **10**, 57 (2018).
33. Wang, X., Ding, B., Yu, J. & Wang, M. Engineering biomimetic superhydrophobic surfaces of electrospun nanomaterials. *Nano Today* **6**, 510–530 (2011).

34. Ding, B., Wang, M., Wang, X., Yu, J. & Sun, G. Electrospun nanomaterials for ultrasensitive sensors. *Mater. Today* **13**, 16–27 (2010).
35. Lutolf, M. & Hubbell, J. Synthetic biomaterials as instructive extracellular microenvironments for morphogenesis in tissue engineering. *Nat. Biotechnol.* **23**, 47–55 (2005).
36. Kim, T. G., Shin, H. & Lim, D. W. Biomimetic scaffolds for tissue engineering. *Adv. Func. Mater.* **22**, 2446–2468 (2012).
37. Yang, F., Murugan, R., Wang, S. & Ramakrishna, S. Electrospinning of nano/micro scale poly (L-lactic acid) aligned fibers and their potential in neural tissue engineering. *Biomaterials* **26**, 2603–2610 (2005).
38. Huang, C. *et al.* The involvement of integrin $\beta 1$ signaling in the migration and myofibroblastic differentiation of skin fibroblasts on anisotropic collagen-containing nanofibers. *Biomaterials* **33**, 1791–1800 (2012).
39. Xie, J. *et al.* Radially aligned, electrospun nanofibers as dural substitutes for wound closure and tissue regeneration applications. *ACS Nano* **4**, 5027–5036 (2010).
40. Wan, L. S. & Xu, Z. K. Polymer surfaces structured with random or aligned electrospun nanofibers to promote the adhesion of blood platelets. *J. Biomed. Mater. Res. A* **89**, 168–175 (2009).
41. Wang, X., Ding, B. & Li, B. Biomimetic electrospun nanofibrous structures for tissue engineering. *Mater. Today* **16**, 229–241 (2013).
42. Yamasaki, J. *et al.* Analysis of nonlinear intensity attenuation in bright-field TEM images for correct 3D reconstruction of the density in micron-sized materials. *J. Electron Microsc.* **63**, 345–355 (2014).
43. Maleki Dizaj, S., Lotfipour, F., Barzegar-Jalali, M., Zarrintan, M.-H. & Adibkia, K. Application of Box–Behnken design to prepare gentamicin-loaded calcium carbonate nanoparticles. *Artif. Cells Nanomed. Biotechnol.* **44**, 1475–1481 (2016).
44. Maleki Dizaj, S., Lotfipour, F., Barzegar-Jalali, M., Zarrintan, M.-H. & Adibkia, K. Ciprofloxacin HCl-loaded calcium carbonate nanoparticles: preparation, solid state characterization, and evaluation of antimicrobial effect against *Staphylococcus aureus*. *Artif. Cells Nanomed. Biotechnol.* **45**, 535–543 (2017).
45. López-Pérez, P. M., da Silva, R. M., Serra, C., Pashkuleva, I. & Reis, R. L. Surface phosphorylation of chitosan significantly improves osteoblast cell viability, attachment and proliferation. *J. Mater. Chem.* **20**, 483–491 (2010).
46. Kumar, D. *et al.* Polarization of hydroxyapatite: Influence on osteoblast cell proliferation. *Acta Biomater.* **6**, 1549–1554 (2010).
47. Anselme, K. Osteoblast adhesion on biomaterials. *Biomaterials* **21**, 667–681 (2000).
48. Farias, S. & Boateng, J. S. Development and functional characterization of composite freeze dried wafers for potential delivery of low dose aspirin for elderly people with dysphagia. *Int. J. Pharm.* **553**, 65–83 (2018).
49. Shahat, A. A., Mahmood, H. M., A-Mishari, A. A. N. A. & Bari, A. Polymers encapsulated aspirin loaded silver oxide nanoparticles: Synthesis, characterization and its bio-applications. *Sains Malaysiana* **48**, 1887–1897 (2019).
50. Hammad, R. *et al.* Multistage release matrices for potential antiplatelet therapy: Assessing the impact of polymers and Sorb-Cel M[®] on floating, swelling, and release behavior. *J. Drug Deliv. Sci. Technol.* **55**, 101387 (2020).
51. Soumya, K., Snigdha, S., Sugathan, S., Mathew, J. & Radhakrishnan, E. Zinc oxide–curcumin nanocomposite loaded collagen membrane as an effective material against methicillin-resistant coagulase-negative *Staphylococci*. *3 Biotech* **7**, 238 (2017).
52. El-Rahman, S. & Al-Jameel, S. Protection of curcumin and curcumin nanoparticles against cisplatin induced nephrotoxicity in male rats. *Sch. Acad. J. Biosci* **2**, 214–223 (2014).
53. Rachmawati, H., Yanda, Y. L., Rahma, A. & Mase, N. Curcumin-loaded PLA nanoparticles: Formulation and physical evaluation. *Sci. Pharm.* **84**, 191–202 (2016).
54. Chen, Z., Mo, X., He, C. & Wang, H. Intermolecular interactions in electrospun collagen–chitosan complex nanofibers. *Carbohydr. Polym.* **72**, 410–418 (2008).
55. Basnett, P. *et al.* Aspirin-loaded P(3HO)/P(3HB) blend films: Potential materials for biodegradable drug-eluting stents. *Bioinspir Biomimetic Nanobiomater.* **2**, 141–153 (2013).
56. Atallah, A. *et al.* Aspirin for prevention of preeclampsia. *Drugs* **77**, 1819–1831. <https://doi.org/10.1007/s40265-017-0823-0> (2017).
57. Fu, K., Griebenow, K., Hsieh, L., Klibanov, A. M. & Langer, R. FTIR characterization of the secondary structure of proteins encapsulated within PLGA microspheres. *J. Control. Rel.* **58**, 357–366 (1999).
58. Santos, M. H. *et al.* Extraction and characterization of highly purified collagen from bovine pericardium for potential bioengineering applications. *Mater. Sci. Eng. C* **33**, 790–800 (2013).
59. Göpferich, A. Mechanisms of polymer degradation and erosion. *Biomaterials* **17**, 103–114 (1996).
60. Gopal, J., Muthu, M. & Chun, S. Bactericidal property of macro-, micro- and nanocurcumin: An assessment. *Arab. J. Sci. Eng.* **41**, 2087–2093 (2016).
61. Ngwabebhoh, F. A., Erdagi, S. I. & Yildiz, U. Pickering emulsions stabilized nanocellulosic-based nanoparticles for coumarin and curcumin nanoencapsulations: In vitro release, anticancer and antimicrobial activities. *Carbohydr. Polym.* **201**, 317–328 (2018).
62. Adahoun, M. A. A., Al-Akhras, M.-A. H., Jaafar, M. S. & Bououdina, M. Enhanced anti-cancer and antimicrobial activities of curcumin nanoparticles. *Artif. Cells Nanomed. Biotechnol.* **45**, 98–107 (2017).
63. Cao, Y. *et al.* Aspirin promotes bone marrow mesenchymal stem cell-based calvarial bone regeneration in mini swine. *Stem Cell Res. Ther.* **6**, 1–11 (2015).
64. Attari, F. *et al.* Curcumin as a double-edged sword for stem cells: Dose, time and cell type-specific responses to curcumin. *DARU J. Pharm. Sci.* **23**, 33 (2015).
65. Barati, D. *et al.* Spatiotemporal release of BMP-2 and VEGF enhances osteogenic and vasculogenic differentiation of human mesenchymal stem cells and endothelial colony-forming cells co-encapsulated in a patterned hydrogel. *J. Control. Release* **223**, 126–136 (2016).
66. Yuan, M. *et al.* Aspirin promotes osteogenic differentiation of human dental pulp stem cells. *Int. J. Mol. Med.* **42**, 1967–1976 (2018).
67. Gu, Q., Cai, Y., Huang, C., Shi, Q. & Yang, H. Curcumin increases rat mesenchymal stem cell osteoblast differentiation but inhibits adipocyte differentiation. *Pharmacogn. Mag.* **8**, 202 (2012).
68. Thirunavukkarasu, K. *et al.* The osteoblast-specific transcription factor Cbfa1 contributes to the expression of osteoprotegerin, a potent inhibitor of osteoclast differentiation and function. *J. Biol. Chem.* **275**, 25163–25172 (2000).
69. Franceschi, R. T. & Xiao, G. Regulation of the osteoblast-specific transcription factor, Runx2: Responsiveness to multiple signal transduction pathways. *J. Cell. Biochem.* **88**, 446–454 (2003).
70. Ryoo, H.-M., Lee, M.-H. & Kim, Y.-J. Critical molecular switches involved in BMP-2-induced osteogenic differentiation of mesenchymal cells. *Gene* **366**, 51–57 (2006).
71. Temenoff, J. S. *et al.* In vitro osteogenic differentiation of marrow stromal cells encapsulated in biodegradable hydrogels. *J. Biomed. Mater. Res. A* **70**, 235–244 (2004).
72. Komori, T. Regulation of bone development and extracellular matrix protein genes by RUNX2. *Cell Tissue Res.* **339**, 189 (2010).
73. Hosseini, F. S. *et al.* Efficient osteogenic differentiation of the dental pulp stem cells on β -glycerophosphate loaded polycaprolactone/polyethylene oxide blend nanofibers. *J. Cell Physiol.* **234**, 13951–13958 (2019).
74. Mirzaei, A. *et al.* Synergistic effects of polyaniline and pulsed electromagnetic field to stem cells osteogenic differentiation on polyvinylidene fluoride scaffold. *Artif. Cells Nanomed. Biotechnol.* **47**, 3058–3066 (2019).

Acknowledgements

This article was written based on a dataset from two theses registered at Tabriz University of Medical Sciences, Faculty of Dentistry (thesis numbers: 36191 and 64206). The theses were performed on Dental and Periodontal Research Center, Tabriz University of Medical Sciences that is greatly acknowledged. The Vice-Chancellor for

Research at Tabriz University of Medical Sciences provided financial support for this research that is greatly acknowledged.

Author contributions

M.G. and A.B. have made an equal contribution to the research steps or the drafting and the editing of the manuscript. They should be considered as co-first authors. M.M. contributed in the microbial section. S.J. contributed in animal operation and processing. S.M. and S.S. had contribution to the all research steps and drafting and scientifically revision of the manuscript. They are the corresponding authors of the manuscript. All authors read and approved the final manuscript.

Competing interests

The authors declare no competing interests.

Additional information

Supplementary information is available for this paper at <https://doi.org/10.1038/s41598-020-75454-2>.

Correspondence and requests for materials should be addressed to S.M.D. or S.S.

Reprints and permissions information is available at www.nature.com/reprints.

Publisher's note Springer Nature remains neutral with regard to jurisdictional claims in published maps and institutional affiliations.



Open Access This article is licensed under a Creative Commons Attribution 4.0 International License, which permits use, sharing, adaptation, distribution and reproduction in any medium or format, as long as you give appropriate credit to the original author(s) and the source, provide a link to the Creative Commons licence, and indicate if changes were made. The images or other third party material in this article are included in the article's Creative Commons licence, unless indicated otherwise in a credit line to the material. If material is not included in the article's Creative Commons licence and your intended use is not permitted by statutory regulation or exceeds the permitted use, you will need to obtain permission directly from the copyright holder. To view a copy of this licence, visit <http://creativecommons.org/licenses/by/4.0/>.

© The Author(s) 2020